https://doi.org/10.1016/j.jmmm.2019.03.001

Tuning ferromagnetic properties of $LaMnO_3$ films by oxygen vacancies and strain

Y. K. Liu, H.F. Wong, K.K. Lam, C.L. Mak and C.W. Leung[1]
Department of Applied Physics, The Hong Kong Polytechnic University, Hum Hom, Hong Kong, China

Abstract

We systematically investigated the ferromagnetic properties of $LaMnO_3$ (LMO) films grown on $SrTiO_3$ (STO) substrates with varying deposition oxygen pressure P_{O2} ($0.2 \leq P_{O2} \leq 200$ mTorr). It was found that the films only deposited with $P_{O2} \leq$ 20 mTorr showed exchange bias behavior and meantime the coercive field H_C of LMO films deposited below 20 mTorr is about one order of magnitude larger than that of films deposited at 200 mTorr. When the LMO films were deposited at 20 mTorr on different substrates [$LaAlO_3$ (LAO), $(LaAlO_3)_{0.3}(Sr_2AlTaO_6)_{0.7}$ (LAST), $SrTiO_3$ (STO) and $KTaO_3$], LMO/STO sample showed the maximum H_C, even though all of them exhibit exchange bias behavior. Thickness dependence of magnetic properties in LMO/STO films deposited at 20 mTorr indicated a maximum coercive field and the existence of exchange bias for 20 nm-thick LMO sample. Based on our results, the enhancement of coercive field and exchange bias was attributed to the competition between different magnetic phases induced by oxygen vacancies and Jahn-Teller effect from strain-induced orbital ordering.

* Electronic mail: dennis.leung@polyu.edu.hk

Introduction

Perovskite manganites, as one of the well-known strongly-correlated electron systems, have raised strong interest for their novel electronic and magnetic properties, due to the complex interaction among the spin, orbital, charge and lattice degrees of freedom and a variety of potential applications in sensors and memories [1-4]. Intriguing physical properties of perovskite manganites (such as metal-insulator transition, ferromagnetic-paramagnetic transition, colossal magnetoresistance, phase separation, as well as charge/orbital ordering) are very sensitive to external stimuli (magnetic field, electric field, doping level, strain and so on). This allows a lot of schemes to manipulate the physical properties and interface coupling in manganite systems [5-11].

The parent compound of $LaMnO_3$ (LMO) has been as a prototypical manganite for investigating the interface coupling when adjoined to other complex oxides [12-16]. Although showing A-type antiferromagnetic (AF) insulating ground state in bulk [17], LMO thin films in heterostructures always exhibit ferromagnetic (FM) behavior [12-16]. This unexpected FM behavior has gained renewed interests, and there are many attempts to explain it.

It was initially suggested that the oxygen pressure during the LMO film growth plays a key role in its FM behavior, which would change the valance of Mn ions and resulting in a 3+/4+ mixed valance state [18-23]. However, x-ray absorption spectroscopy measurements in LMO/LSAT thin films deposited at low oxygen pressure indicated the existence of Mn^{2+} component associated with the double-exchange between Mn^{2+}-O-Mn^{3+},which gives rise to exchange bias [24]. On the other hand, strain effect due to lattice mismatching between film and substrate materials also plays a crucial role in the properties of the resultant films. Theoretical studies indicated that the FM behavior in LMO thin films originates from the strain-induced orbital ordering [25-27]. Experimentally, LMO films grown on $LaAlO_3$ (LAO) substrates with decreasing thickness demonstrated an increasing FM transition temperature [28]. Meanwhile, it was reported that by reducing the growth oxygen pressure, LMO thin films deposited on $SrTiO_3$ (STO) substrates can be tuned from FM to AF due to the strain-induced orbital ordering [29]. Therefore, in spite of reports which investigated the effects of oxygen pressure on the magnetic properties of LMO thin films, the relation between magnetism with oxygen pressure and strain is still unclear. Besides, whether one

can realize two different magnetic phases coexisting in LMO film is also unknown, and further investigations awaits along this direction [30].

As an attempt to address some of the previously mentioned issues, in this work we fabricated a series of LMO thin films on STO substrates with different oxygen pressures (P_{O2}) and systematically studied their microstructures and magnetic properties. From x-ray diffraction measurements, we found that the out-of-plane lattice parameter increased with decreasing P_{O2}. LMO/STO films deposited at low P_{O2} (20, 2 and 0.2 mTorr) showed obvious enhancement of coercivity (H_C), reaching up to 30 times that of LMO film deposited at 200 mTorr. On the other hand, exchange bias (EB) effect was observed in LMO/STO samples with $P_{O2} \leq 20$ mTorr. Minor loop measurements for samples with $P_{O2} \leq 20$ mTorr revealed the presence of two FM phases with different H_C. When the LMO films were deposited at 20 mTorr on different substrates [LAO, $(LaAlO_3)_{0.3}(Sr_2AlTaO_6)_{0.7}$, STO and $KTaO_3$], we found the LMO/STO sample showed the largest H_C. From the thickness dependence of magnetic properties of LMO/STO films deposited at 20 mTorr, it was found that the 20 nm-thick LMO sample exhibited a maximum H_C and EB. Our results indicated that the competition between different magnetic phases induced by oxygen vacancies, and Jahn-Teller effect from strain-induced orbital ordering, should play key roles in the magnetic properties of LMO films.

Experimental details

A series of epitaxial LMO thin films with different thicknesses were grown by pulsed laser deposition with a laser wavelength of 248 nm on various substrates, using a stoichiometric LMO target. The frequency and energy of the excimer laser were 2 Hz and 1.5 Jcm^{-2}, respectively. The film growth took place at a substrate temperature of 710˚C under different P_{O2} in the range of 0.2 to 200 mTorr. After the deposition, the samples were cooled down to room temperature naturally under the same oxygen pressure environment.

Crystal structure of the films was characterized by high-resolution X-ray diffractometery (Smartlab, Rigaku, Japan). Magnetic properties of the samples were measured by vibrating sample magnetometery (VSM, Quantum Design). For the field-cooled (FC) magnetization-temperature measurements, samples were cooled down from 300 K to 3 K under an applied magnetic field of 1 kOe, and

were then measured under the same field during the warming process. The magnetic hysteresis loops (*M-H* loops) were measured after FC the samples from 300 K to the desired temperatures under a 2 T magnetic field.

Results and discussions

Oxygen Dependence of Magnetic Properties. Fig. 1 shows the XRD profile of the LMO films (30 nm) at different P_{O2}, which shows clear (001) LMO peaks and is indicative of the high crystallinity and *c*-axis orientation. Laue fringes were observed around the (001) diffraction peak, which further suggests the high quality of the films. Remarkably, with decreasing P_{O2} from 200 to 2 mTorr, the (001) peak position shifts to lower angles, indicating an expansion of the out-plane lattice constant *c* (inset of Fig.1). As for the stoichiometric bulk LMO, the pseudocubic lattice parameter (a ~ 3.93 Å [31]) is similar to that of LMO film deposited at 200 mTorr, which indicates that the LMO/STO deposited below 20 mTorr are under compressive strain. According to the reported results [32], the expansion of lattice constant could be attributed to the effect of oxygen vacancies, which weakens the lattice interatomic force and change the valence of Mn ions. By considering the Mn ionic radii at different valence states (Mn^{2+} (0.83Å), Mn^{3+}(0.645Å) and Mn^{4+}(0.53Å)) [24, 33] and the above results, it is likely that the Mn^{2+} has appeared other than Mn^{4+} with decreasing oxygen pressure, which was verified in LMO/LSAT films [24].

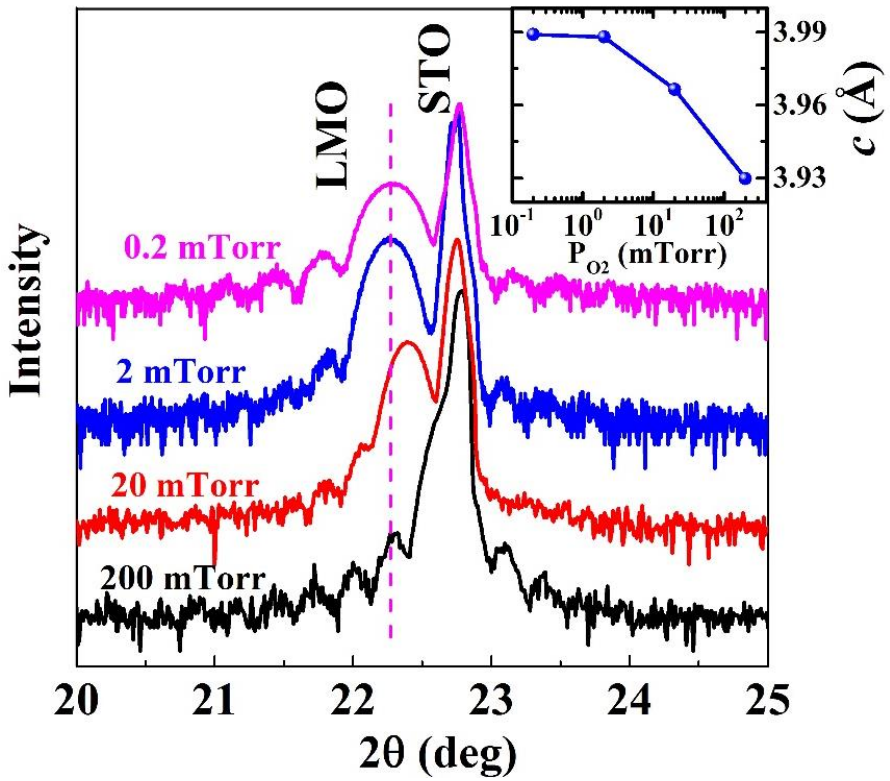

FIG.1. XRD profile showing (001) peak of LMO films grown on (001) STO substrates at different P_{O2}. The dashed line is a guide to the eyes. Inset shows the P_{O2} dependence of the out-plane lattice constant *c* as extracted from the LMO (001) peak.

Magnetic properties of LMO/STO thin films as a function of P_{O2} are shown in Fig.2. The FC magnetization-temperature (*M*-*T*) curves for samples deposited at different P_{O2} are plotted in Fig.2a, with both FC and measurement fields being 1 kOe. It is obvious that the Cure temperature (T_C) of the LMO film decreases when P_{O2} drops from 200 mTorr to 20 mTorr, which is the same as those reported in literature [18, 22, 34]. With further decreasing P_{O2}, T_C does not show any variations. As for the sample deposited at 200 mTorr, the *M*-*H* loop shows a robust FM behavior with H_C of 280 Oe at 3 K (inset of Fig.2a), with $H_C = (H_2-H_1)/2$ where H_1 and H_2 are the negative and positive fields at which the magnetization equals zero. It should be noted that the *M*-*H* loops in the present work were measured with a 2-T field cooling from 300 K to the desired temperatures.

We also attempted to evaluate the presence of exchange coupling effect by measuring the EB field ($H_{EB}=(H_1+H_2)/2$). No exchange bias effect was found in LMO/STO sample deposited at 200 mTorr, which is different from the reported LMO films grown on LSAT substrates [24]. As the P_{O2} decreases to 20 mTorr, one

can find the *M-H* loop at 3 K (Fig. 2(b)) exhibits a much higher H_C (4580 Oe) than that of the film deposited at 200 mTorr (inset of Fig.2a). Another visible feature of the *M-H* loop in Fig.2(b) is the loop shift towards the negative field, which is a manifestation of the EB. At 3 K, H_{EB} of the LMO film deposited at 20 mTorr is about 105 Oe. Even higher H_C and H_{EB} can be found in films grown under lower P_{O2} (Fig. 2(c) for P_{O2} = 2 mTorr, and Fig.2(d) for P_{O2} = 0.2 mTorr). Such observations of H_C enhancement and H_{EB} confirm that the exchange bias is intrinsic for LMO thin films deposited under low P_{O2} ($\leq$ 20 mTorr) and measured at low temperatures. The EB behavior in LMO thin film suggests the presence of multiple phases with different spin orders, which couples with each other and results in EB.

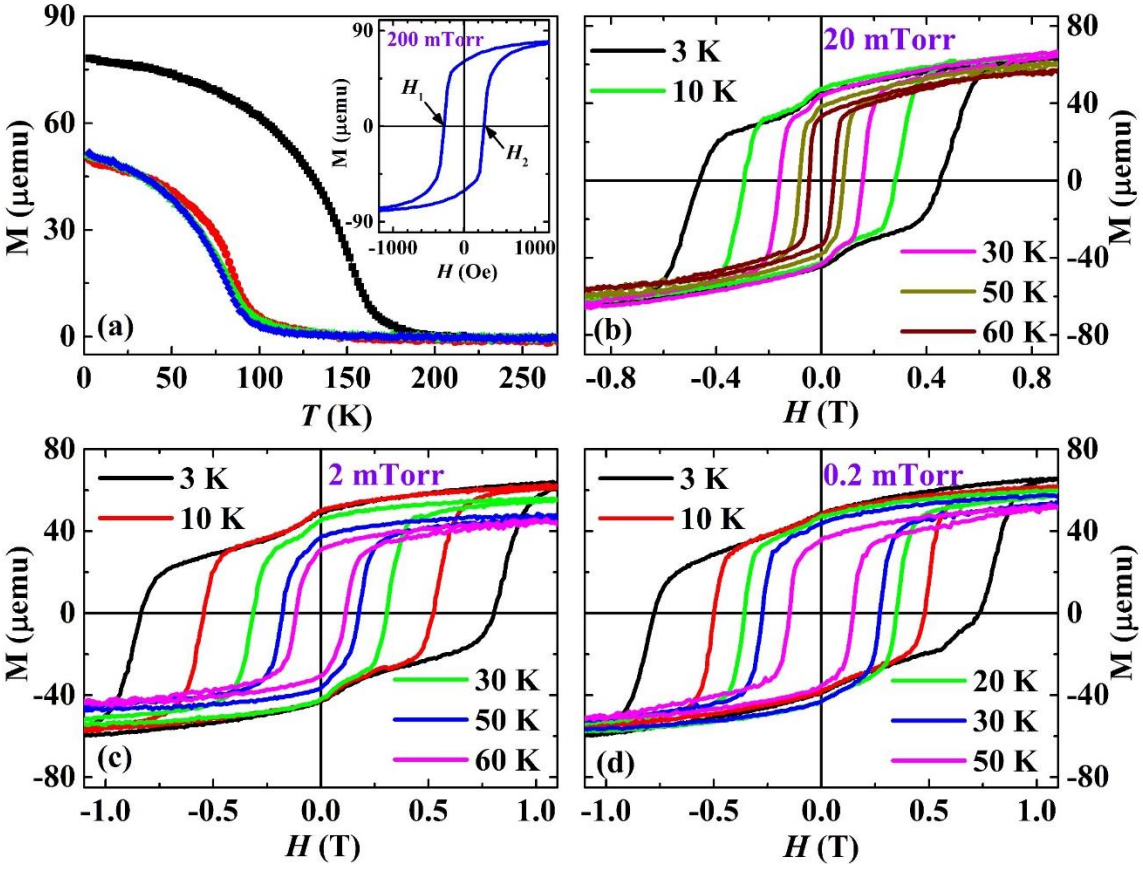

FIG.2. (a) *M-T* curves of LMO films deposited at different P_{O2} and measured after 1 kOe field cooling: 200 mTorr (black), 20 mTorr (red), 2 mTorr (green), 0.2mTorr (blue). Inset shows the *M-H* loop of LMO film deposited at 200 mTorr at 3 K. (b)-(d) *M-H* loops of LMO films deposited at P_{O2} = 20 mTorr (b), 2 mTorr (c) and 0.2mTorr (d) and measured at different temperatures. All the *M-H* loops were measured after 2T field cooling from 300 K.

As reported in literature [35-37], with increasing temperature H_C and H_{EB} decrease and H_{EB} vanishes at the blocking temperature (T_B). In Fig. 3 we summarize the temperature dependence of H_C and H_{EB} for LMO films deposited with different P_{O2}. For all LMO samples studied, H_C drops monotonously with increasing temperature and approaches zero at around 90 K, which is T_C as determined from $M(T)$ (Fig. 2a). We point out that H_C increases up to about 30 times with decreasing P_{O2} (from 280 Oe for P_{O2} = 200 mTorr to 8200 Oe for P_{O2} = 2 mTorr) as shown in Fig.3(c). As for the H_{EB} (Fig.3(b)), it abruptly decays with increasing temperature and disappears at T_B [38, 39] about 50 K for the samples with $P_{O2} \leq 20$ mTorr (Fig.3(b)). It is noticeable that T_B is a little smaller than the T_C. Indeed, the competing magnetic interactions is known to lead to an exponential temperature-dependent decay of H_C and H_{EB}, which has previously been observed in $La_{0.7}Sr_{0.3}MnO_3/SrMnO_3$ bilayers [40], $La_{1-x}Ca_xMnO_3$ ferromagnetic/ antiferromagnetic multilayers [36] and $La_{0.7}Sr_{0.3}MnO_3$ nanoparticles [41]. The temperature dependences of H_C and H_{EB} can be fitted by the phenomenological formulae [36, 40]

$$H_C = H_C(0)\exp(-T/T_1)$$
$$H_{EB} = H_{EB}(0)\exp(-T/T_2), \qquad (1)$$

where $H_C(0)$ and $H_{EB}(0)$ are the extrapolations of H_C and H_{EB} to absolute zero, and T_1 and T_2 are constants. The fitting results (solid lines in Figs.3(a) and 3(b)) indicate there should exist different magnetic phases in LMO films when deposited at low oxygen pressures. With increasing P_{O2}, H_{EB} firstly decreases and then almost keeps constant, which is similar to the variation of H_C as shown in Fig.3(c). Obviously, H_C and H_{EB} show the similar variation with decreasing P_{O2}.

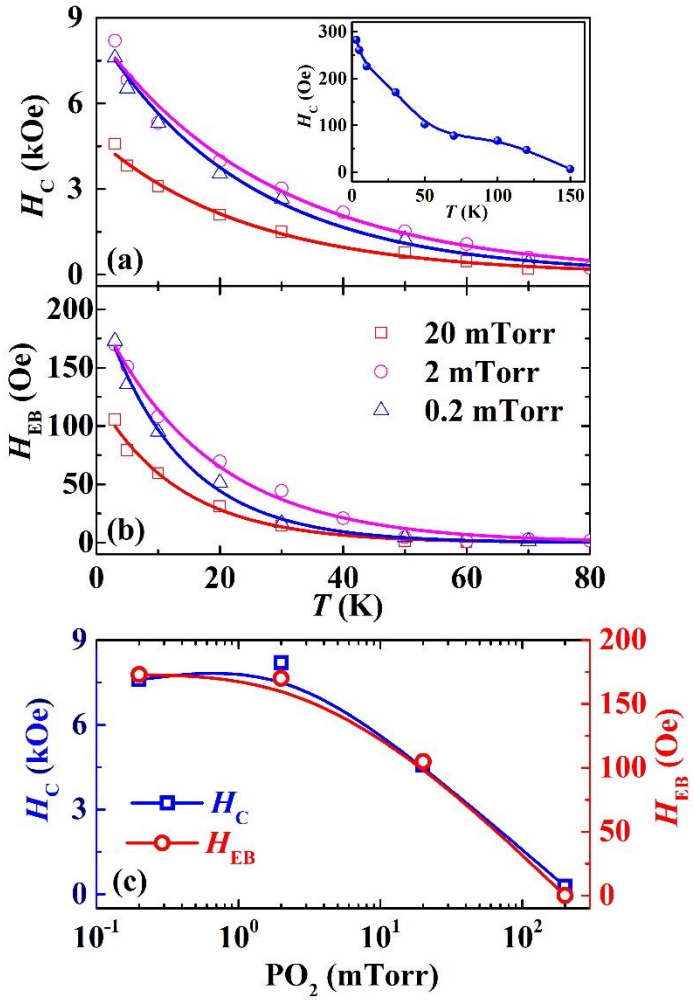

Fig.3. (a) Temperature dependence of H_C of LMO thin films deposited at 200 mTorr (inset), 20 mTorr (red squares), 2 mTorr (green triangles) and 0.2mTorr (blue circles). (b) H_{EB} as a function of temperature with different P_{O2}. The solid lines in (a) and (b) are the fits using Eq.(1). (c) The deposited oxygen pressure P_{O2} dependence of H_C and H_{EB}.

Apart from the enhancement of H_C and EB, the most outstanding feature of low-temperature *M-H* loops for LMO films deposited with low P_{O2} is a distinct kink at low magnetic field range (c.f. Fig. 2). Such a behavior indicates the possible existence of another FM phase with lower H_C. The coexistence of two phases of magnetic materials with different H_C would lead to the exchange spring effect [42, 43], which has been studied in heterogeneous hard/soft FM bilayers such as $Ni_{80}Fe_{20}/Sm_{40}Fe_{60}$ [37], CoCr/CoPtCrB [44], and $La_{0.7}Sr_{0.3}CoO_3/La_{0.7}Sr_{0.3}MnO_3$ [45]. As for the manganites, the phase separation with the coexistence of different magnetic phases in a single system provides "homo-interfaces" and resulting in numerous fascinating phenomena [24, 46, 47]. In particular, the electronic phase

separation in LMO bulk [48] and films [24] have been confirmed, typically accompanied by different magnetic phases. On the other hand, the exchange spring effect has been observed in bulk $Pr_{1-x}Ca_xCoO_3$ [30], where the long-range ordered FM phase (low H_C) coexists spatially with a short-range FM phase (high H_C), indicating two different FM phases can coexist in a single material system.

Based on the above discussions, we deduce that the LMO thin films deposited with $P_{O2} \leq 20$ mTorr contain two FM phases with different H_C, and the exchange spring effect between these two FM phases could explain the observed EB. In order to characterize the second FM part with lower H_C in details, we measured the minor hysteresis loop at 3 K for the LMO/STO sample with P_{O2} = 20 mTorr (Fig. 4). For extracting the minor loop I, a magnetic field up to 2 T was first applied, and then the field was swept down to -2000 Oe before it was ramped up back to 3000 Oe. A clear minor loop is observed, which shows a smaller saturation magnetization and a lower H_C compared with the major loop. Similar minor loop behavior can be observed when the field is swept from –2 T, reversed at 2000 Oe and then ramped up again at –3000 Oe until the major loop is completed when the field reaches 2 T. The H_C of minor loops (defined at fields where the magnetization equals to the half of the sum of the moment at A and B in Fig. 4) are about 510 Oe (loop I) and 540 Oe (loop II), which are similar to that of LMO film deposited at P_{O2} = 200 mTorr (Fig.2) and much smaller than that in the major loop.

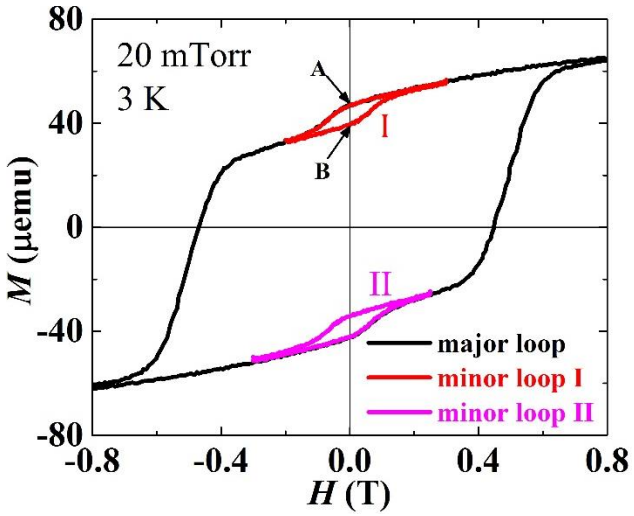

Fig.4. Major and minor loop measurements at 3 K, for LMO thin film deposited at 20 mTorr. See text for the field sequences used to obtain the loops.

Substrates Dependence of Magnetic Properties in LMO. To further investigate the unusual magnetic behavior of LMO films at low P_{O2}, a series of LMO films with thickness 24 nm were deposited on (001)-oriented LAO (lattice parameter a = 3.793Å), LSAT (3.868Å), STO (3.905Å) and KTO (3.989Å) single crystal substrates at 20 mTorr. Noting the pseudocubic lattice parameter of stoichiometric LMO bulk is a ~3.93 Å [31], hence LMO films will be closely matched with STO compared to others substrates, but suffer from out-of-plane tensile stress on LAO and LSAT, and compressive stress on KTO. This is verified from the XRD profiles in Fig. 5(a), which show epitaxial growth of LMO films on all the substrates but with strongly tensile, moderately tensile, weakly tensile, and strongly compressive strains, respectively. It is known that the magnetic behavior of LMO films is closely related to the substrate-induced strains [25], as the epitaxial strain influences the oxygen-octahedron rotation and Jahn-Teller distortion which will play an important role on the magnetic behavior of manganite films [49].

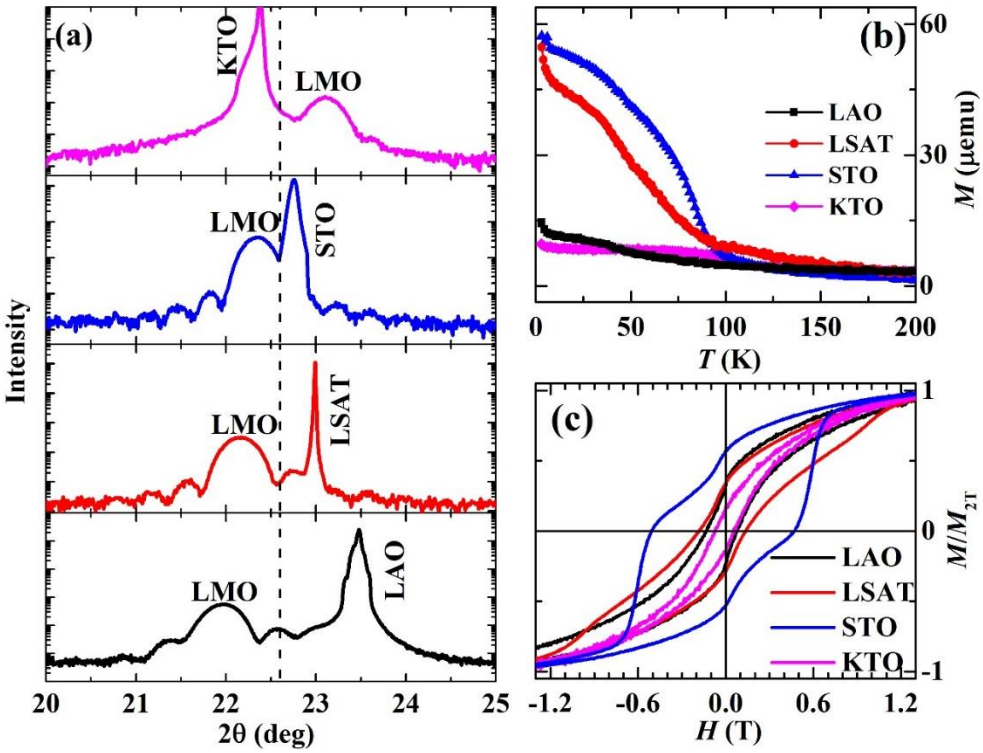

Fig.5 (a) X-ray diffraction θ-2θ scans of LMO films on LAO, LSAT, STO and KTO. The dashed line indicates the position of the bulk LMO 2θ value. (b) Field-cooled magnetization vs. temperature for LMO films. Both the field cooling and measuring fields were 1 kOe. (c) Magnetic hysteresis loops of LMO/LAO, LMO/LSAT, LMO/STO and LMO/KTO films at 3 K. All the samples were cooled from 300 K to 3 K at a field of 2 T.

Fig. 5(b) exhibits the field cooling *M-T* curves of LMO films, upon cooling field and measuring field with an external field of 1 kOe. The magnetization of LMO films under strongly compressive or tensile strains are much smaller below 100 K, and the magnetization of LMO/LSAT is slight smaller than that of LMO/STO. This temperature dependence of magnetization for LMO films deposited at 20 mTorr is consistent with the strain state of LMO films on different substrates, i.e. when the LMO film is slightly strained it shows robust ferromagnetic behavior, and the compressive or tensile strain will result in the progressive reduction of magnetization in LMO film. First-principles calculations [26, 50] and experiments [51] indicated that as the compressive or tensile strains of LMO film induced by different substrates increase, the ferromagnetism of LMO film will be more strongly suppressed. Ferromagnetism of film is found to be stable in a small tensile strain range according to the calculations [26, 50]. That is similar to our data for LMO films grown on different substrates. As regards the orbital ordering, calculations [26] indicated that the compressive strain LMO will show x^2-1/y^2-1 orbital ordering, while tensile strain will result in (x^2-y^2)+(z^2-1) orbital ordering only which will induce FM in LMO films, and then change to z^2-1 ordering with further increasing tensile strain. On the other hand, oxygen octahedral rotation is another nontrivial factor in determining the FM of LMO films when grown on STO [14, 16, 51, 52], in which the strong coupling with Jahn-Teller distortion results in orbital ordering. So even if the mismatch is minimum between LMO and STO, the tensile strain and oxygen octahedral rotation will cause orbital ordering, and give rise to FM in LMO/STO film. Therefore, the interplay between the Jahn-Teller distortion, oxygen octahedral rotation and orbital ordering will cause the complex magnetic behavior of LMO films grown on different substrates.

The most important result on the strain dependences of the magnetic properties is shown in Fig.5 (c), which depicts the hysteresis loops of LMO films on different substrates (hence strain states) at 3 K; all the samples were field cooled in a 2 T external field from 300 K to 3 K. It can be seen that the shape of *M-H* loops of highly-stressed LMO films (with LAO, LSAT and KTO) are much slenderer than that deposited on STO, and only in LMO/STO are the H_C enhancement and the "kinked" behavior in *M-H* loop observed. As when we plot the substrate lattice

dependence of H_C and H_{EB} (Fig.6), H_{EB} decreases with increasing substrate lattice parameter, while H_C peaks at the lattice parameter of STO and then decreases.

The maximum H_C in LMO/STO sample can be explained by the appearance of second FM part with higher H_C, which may only be found when the lattice of film matches well with the substrate. With strong tensile or compressive strains, the FM state in LMO films grown at 20 mTorr will be suppressed, and AF ordering will appear and become the dominant phase in LMO film, which would result in the decrement of magnetic moment and H_C and a much slender *M-H* loop. The mechanism of the strain dependence of the magnetic ordering and the coupling among them in LMO film deposited at 20 mTorr is complex and can related to the effects of strain-induced magnetic phase transition, Jahn-Teller distortion, and oxygen-octahedron rotation [49], which need be further investigated by experiments and theory.

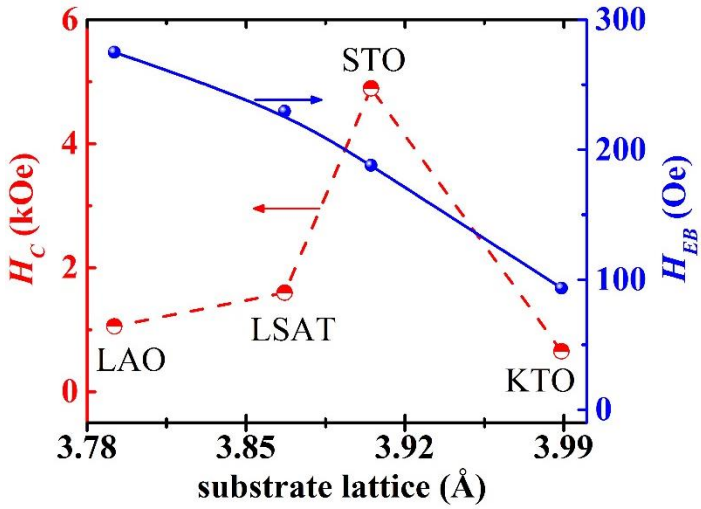

Fig.6 The substrate lattice dependence of the H_C and H_{EB}.

Another interesting point for *M-H* loops in Fig. 5(c) is the presence of distinct kink at low magnetic field range, which is particularly prominent in LMO/STO sample. In order to further study this behavior, we measured a series of *M-H* minor loops for this sample at 3 K (Fig.7(a). These minor loops were obtained by firstly saturating the sample with +2 T, then ramping down the field to a value H_r such that the field is increased back to 2 T. For example, in Fig. 7(a) the value of H_r changes gradually from –0.2 T to -0.8 T. For the minor loop with H_r = -0.2 T, the

minor loop is a normal hysteresis loop with H_C ~ 380 Oe. With increasing H_r from -0.2 to -0.6 T, the minor loop opens up. A plot of the normalized minor loop area A_{minor}/A_{major} (A major refers to the complete *M-H* loop measured between ±2 T) as a function of H_r (Fig. 7(b)) shows negligible value for H_r between 0 to -0.3 T, but dramatically rises with higher magnitude of H_r. This is the prototypical exchange-spring behavior [53]. Therefore, the LMO/STO film deposited at 20 mTorr may exhibit two FM phases with different H_c, and the exchange springing between these two FM phases results in the EB.

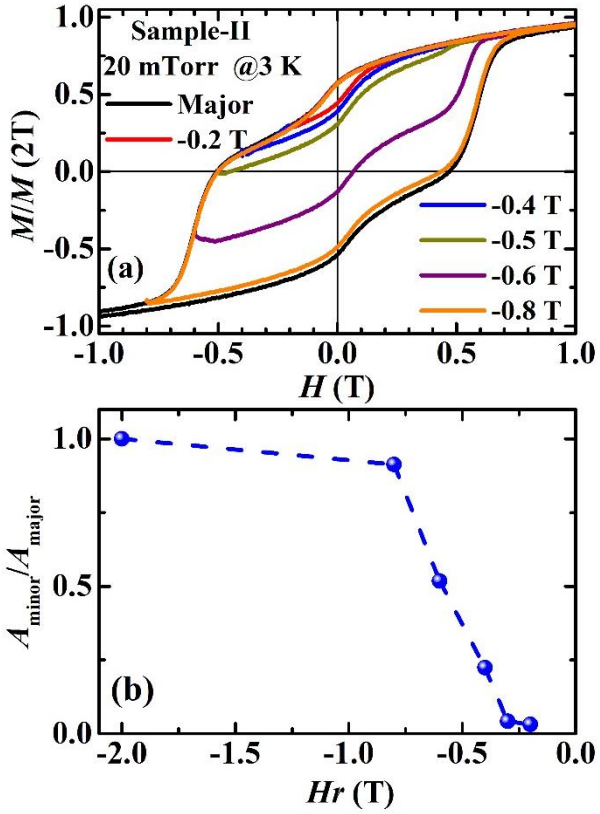

Fig.7. (a) Normalized hysteresis loops (both major and minor loops) at 3 K for LMO/STO deposited with P_{O2} = 20 mTorr. The minor loops were initiated at +2T and labeled with the field H_r in which the field sweeping direction is reversed. (b) H_r dependence of the area of the minor loop normalized to the area of the major loop.

Thickness Dependence of Magnetic Properties. From the results of the LMO films on different substrates deposited at P_{O2} = 20 mTorr, we can see the high sensitivity of the LMO film magnetism on the substrate-induced strain. We therefore further explored the strain effect by preparing LMO films of different

thicknesses (t nm) on STO at 20 mTorr. Fig. 8(a) displays the XRD profiles around (001) peaks for LMO films with $8 \leq t \leq 105$. With t increases up to 38 nm, the diffraction peaks shift to high angles, indicating a gradual strain relaxation of the LMO film. When the film thickness further increases up to 105 nm, no further shifting of diffraction peak can be found. From the thickness dependence of the out-plane parameter c of LMO/STO films (Fig. 8(b)), it is found that c decreases dramatically with increasing thickness up to 38 nm, and is almost constant with further increasing t, suggesting a strain-relaxed LMO/STO film with $t \geq 38$ nm.

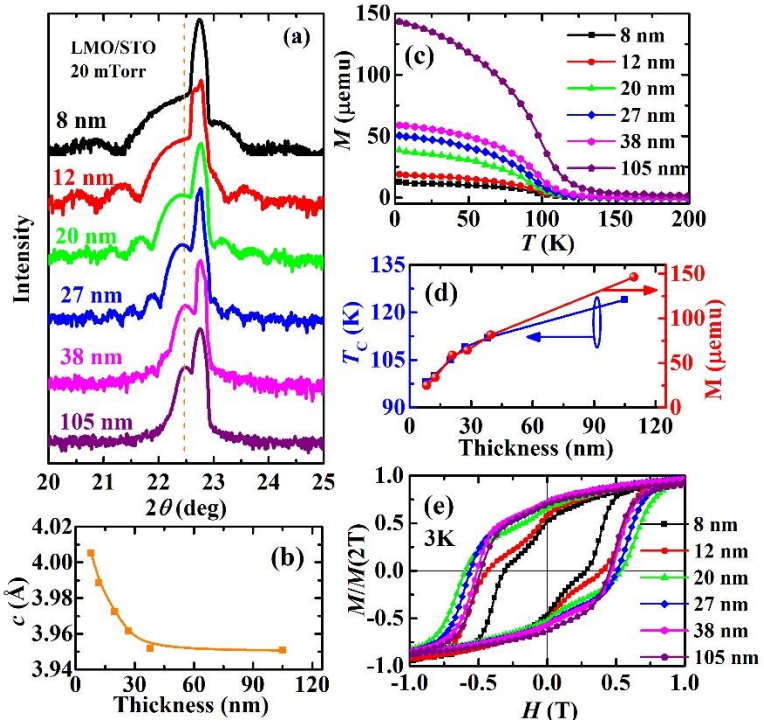

Figure 8. (a) XRD θ-2θ patterns around (001) diffraction of the LMO films on STO substrates with different thickness. Vertical dashed line is guideline for the comparison of the LMO peaks with different thickness. (b) Variation of the out-plane parameter c of LMO/STO films deposited at 20 mTorr as a function of thickness t. (c) M-T curves of LMO films deposited at 20 mTorr with different thickness, after cooling in 1 kOe field and were measured with the same field. (d) Thickness dependence of T_C (blue square) and saturation magnetization M_s (red circle) for the LMO/STO films. (e) Normalized M-H loops of LMO films with different thicknesses, measured at 3 K after field-cooled from 300 K to 3 K in a field of 2 T.

Fig. 8(c) displays the M-T traces of LMO films ($8 \leq t \leq 105$ nm), after field-cooling in 1 kOe and measured in the same fields. It is obvious that the saturation magnetic moment M_s (at 2 T) and transition temperature T_C increase with rising t. In order to see clearly the thickness-dependent variation of T_C and M_s, we

summarize the results in Fig. 8(d), where T_C and M_s show the same variation with increasing thickness. Obviously, below t = 27 nm, the increasing rapids of T_C and M_s are little faster than that of above 27 nm samples, indicating the strain plays an important role in its magnetic properties.

Fig. 8(e) exhibits the normalized *M-H* loops of LMO films of different thicknesses at 3 K, after field cooling the samples in 2 T from room temperature to 3 K. Importantly, all the LMO/STO samples show H_{EB}, enhanced H_C and a kink at low magnetic field range (c.f. Figs. 2 and 7). The maximum H_C (collected from the major loop) can be observed in the 20 nm-sample. In Fig. 9 we plot H_C and H_{EB} collected from the major loop of Fig. 8(d) as a function of t, and both of them show the similar variation, i.e. a sharp increase with increasing t, reaching a maximum at 20 nm, and then gradually decrease with larger film thickness. Apparently, the exchange coupling between two FM part of LMO film at 20 nm reaches maximum, resulting in maximal H_C and H_{EB}.

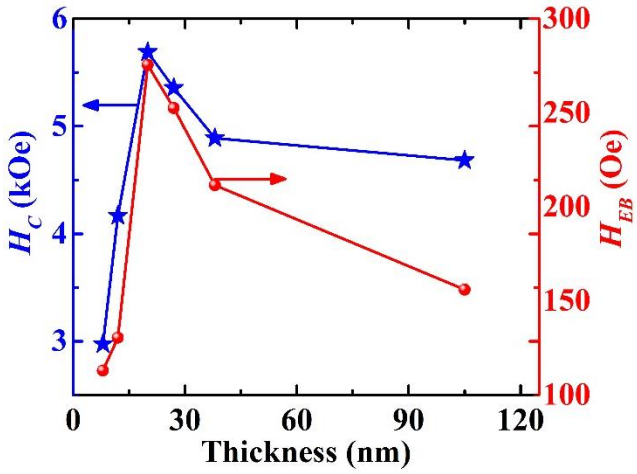

Figure 9. Thickness dependence of H_C and H_{EB} of LMO films deposited at 20 mTorr.

Based on the above results and discussion, we conclude that the magnetic properties of LMO thin films are very sensitive to the P_{O2} and epitaxial strain. At low P_{O2} one can find the enhanced H_C and H_{EB}, as well as a distinct kink in *M-H* loop at low field resulting from different FM components that demonstrate exchange spring effect. One possible explanation is the presence of magnetic phase change [30]. The observed magnetic interaction reaches a maximum at the film thickness of 20 nm. From the study of XRD measurement with P_{O2} (Fig. 1) and previous reported results [24], decreasing P_{O2} leads to the formation of Mn^{2+},

which is associated with the double exchange in Mn^{2+}-O-Mn^{3+} and hence produces robust ferromagnetism. As for the epitaxial strain, it would drive the rotation of the MnO_6 octahedra due to the Jahn-Teller effect [2, 3], and then affects its electronic structure and physics properties [2, 54]. Theoretical investigated on the LMO films also indicated that a large cooperative coupling of Jahn-Teller distortion to oxygen-octahedron rotations has a significant effect on its magnetic property, which can be manipulated by the epitaxial strain [26, 49]. Experiments and theories [14, 16, 25, 27] have confirmed that the FM in LMO/STO film is resulted from the strain induced orbital ordering. According to our results, it further confirms that strain plays an important role in the magnetic and exchange bias of LMO films.

We also note that STO undergoes a phase transition near 100 K from a high temperature cubic to a low temperature tetragonal phase [55, 56]. The twining in the STO substrate in the tetragonal phase will induces twinning domains in manganite films grown on STO [57, 58]. Thus, it may be thought that the effect of structural coupling between LMO and STO may make some contribution to the observed magnetic behavior, which need to be further investigated.

Conclusion

In summary, we systematically studied the tuning of magnetic properties of LMO films by deposited oxygen pressure and strain, and have the following findings.

1) Depositing LMO films on STO substrates with different oxygen pressure P_{O2} indicated that films prepared at low oxygen pressure showed enhancement of H_c and EB effect. H_{EB} decreases with incre $P_{O2} \leq 20$ mTorr show a kink at low field range at low temperature, possibly due to the existence of two different FM phases, and the exchange spring effect between these phases induced exchange bias.

2) Comparing the magnetic properties of LMO films grown on LAO, LSAT, STO and KTO substrates at 20 mTorr, it was found that LMO/STO sample showed maximum H_C, even though all of them exhibit exchange bias.

3) Investigating the thickness dependence of magnetic properties of LMO/STO films deposited at 20 mTorr, we found that LMO/STO always showed enhanced H_C and H_{EB} between 8 nm and 105 nm at 3 K, and at 20 nm both quantities achieved the maximum value.

Our results indicate the magnetic properties of LMO thin film are closely related to the deposited oxygen pressure and substrate, and the enhanced coercive field and exchange bias are attributed to the competition between different magnetic phases induced by oxygen vacancies and strain-induced Jahn-Teller effect.

Acknowledgments

This work was supported by the National Natural Science Foundation of China (Grant No. 51502129), the Hong Kong Research Grant Council (PolyU 153027/17P) and The Hong Kong Polytechnic University (1-ZVGH).

Reference

[1] M.B. Salamon, M. Jaime, The physics of manganites Structure and transport, Rev.Mord. Phys., 73 (2001) 583.
[2] A.-M. Haghiri-Gosnet, J.-P. Renard, CMR manganites physics, thin films and devices, J. Phys. D: Appl. Phys., 36 (2003) R127.
[3] Y.-K. Liu, Y.-W. Yin, X.-G. Li, Colossal magnetoresistance in manganites and related prototype devices, Chin. Phys. B., 22 (2013) 087502.
[4] L.W. Martin, R. Ramesh, Multiferroic and magnetoelectric heterostructures, Acta Mater., 60 (2012) 2449-2470.
[5] Y. Tokura, Critical features of colossal magnetoresistive manganites, Rep. Prog. Phys., 69 (2006) 797-851.
[6] E. Dagotto, T. Hotta, A. Moreo, Colossal magnetoresistant materials the key role of phase separation, Phys. Rep., 344 (2001) 1.
[7] M.B. Lepetit, B. Mercey, C. Simon, Interface effects in perovskite thin films, Phys. Rev. Lett., 108 (2012) 087202.
[8] H. Das, G. Sangiovanni, A. Valli, K. Held, T. Saha-Dasgupta, Size control of charge-orbital order in half-doped manganite La0.5Ca0.5MnO3, Phys. Rev. Lett., 107 (2011) 197202.
[9] N.A. Babushkina, L.M. Belova, O.Y. Gorbenko, A.R. Kaul, A.A. Bosak, V.I. Ozhogin, K.I. Kugel, Metal–insulator transition induced by oxygen isotope exchange in the magnetoresistive perovskite manganites, Nature, 391 (1998) 159.
[10] L.M. Zheng, X.R. Wang, W.M. Lu, C.J. Li, T.R. Paudel, Z.Q. Liu, Z. Huang, S.W. Zeng, K. Han, Z.H. Chen, X.P. Qiu, M.S. Li, S. Yang, B. Yang, M.F. Chisholm, L.W. Martin, S.J. Pennycook, E.Y. Tsymbal, J.M.D. Coey, W.W. Cao, Ambipolar ferromagnetism by electrostatic doping of a manganite, Nat Commun, 9 (2018) 1897.
[11] A. Chen, Z. Bi, Q. Jia, J.L. MacManus-Driscoll, H. Wang, Microstructure, vertical strain control and tunable functionalities in self-assembled, vertically aligned nanocomposite thin films, Acta Mater., 61 (2013) 2783-2792.
[12] S. Smadici, P. Abbamonte, A. Bhattacharya, X. Zhai, B. Jiang, A. Rusydi, J.N. Eckstein, S.D. Bader, J.M. Zuo, Electronic reconstruction at SrMnO3-LaMnO3 superlattice interfaces, Phys. Rev. Lett., 99 (2007) 196404.
[13] J. Garcia-Barriocanal, F.Y. Bruno, A. Rivera-Calzada, Z. Sefrioui, N.M. Nemes, M. Garcia-Hernandez, J. Rubio-Zuazo, G.R. Castro, M. Varela, S.J. Pennycook, C. Leon, J. Santamaria, "Charge leakage" at LaMnO3/SrTiO3 interfaces, Adv. Mater., 22 (2010) 627-632.
[14] J. Garcia-Barriocanal, J.C. Cezar, F.Y. Bruno, P. Thakur, N.B. Brookes, C. Utfeld, A. Rivera-Calzada, S.R. Giblin, J.W. Taylor, J.A. Duffy, S.B. Dugdale, T. Nakamura, K. Kodama, C. Leon, S. Okamoto, J. Santamaria, Spin and orbital Ti magnetism at LaMnO3/SrTiO3 interfaces, Nat. Commun., 1 (2010) 82.
[15] A.B. Shah, Q.M. Ramasse, X. Zhai, J.G. Wen, S.J. May, I. Petrov, A. Bhattacharya, P. Abbamonte, J.N. Eckstein, J.M. Zuo, Probing interfacial electronic structures in atomic layer LaMnO(3) and SrTiO(3) superlattices, Adv. Mater., 22 (2010) 1156-1160.
[16] M. Gibert, P. Zubko, R. Scherwitzl, J. Iniguez, J.M. Triscone, Exchange bias in LaNiO3-LaMnO3 superlattices, Nat. Mater., 11 (2012) 1958.
[17] E.O. Wollan, W.C. Koehler, Neutron Diffraction Study of the Magnetic Properties of the Series of Perovskite-Type Compounds[(1−x)La, xCa]MnO3, Phys. Rev., 100 (1955) 545-563.
[18] H.S. Kim, H.M. Christen, Controlling the magnetic properties of LaMnO3 thin films on SrTiO3(100) by deposition in a O2/Ar gas mixture, J. Phys. Condens. Matter., 22 (2010) 146007.

[19] A. Gupta, T.R. McGuire, P.R. Duncombe, M. Rupp, J.Z. Sun, W.J. Gallagher, G. Xiao, Growth and giant magnetoresistance properties of La-deficient LaxMnO3−δ (0.67≤x≤1) films, Appl. Phys. Lett., 67 (1995) 3494.
[20] T.R. McGuire, A. Gupta, P.R. Duncombe, M. Rupp, J.Z. Sun, R.B. Laibowitz, W.J. Gallagher, G. Xiao, Magnetoresistance and magnetic properties of $La_{1-x}\square_xMnO_{3-\delta}$ thin films, J. Appl. Phys., 79 (1996) 4549.
[21] W.S. Choi, Z. Marton, S.Y. Jang, S.J. Moon, B.C. Jeon, J.H. Shin, S.S.A. Seo, T.W. Noh, K. Myung-Whun, H.N. Lee, Y.S. Lee, Effects of oxygen-reducing atmosphere annealing on LaMnO3epitaxial thin films, J. Phys. D: Appl. Phys., 42 (2009) 165401.
[22] Z. Marton, S.S. A. Seo, T. Egami, H.N. Lee, Growth control of stoichiometry in LaMnO3 epitaxial thin films by pulsed laser deposition, J. Cryst. Growth, 312 (2010) 2923-2927.
[23] M. Takacs, M. Hoes, M. Caduff, T. Cooper, J.R. Scheffe, A. Steinfeld, Oxygen nonstoichiometry, defect equilibria, and thermodynamic characterization of LaMnO 3 perovskites with Ca/Sr A-site and Al B-site doping, Acta Mater., 103 (2016) 700-710.
[24] J.J. Peng, C. Song, B. Cui, F. Li, H.J. Mao, Y.Y. Wang, G.Y. Wang, F. Pan, Exchange bias in a singleLaMnO3film induced by vertical electronic phase separation, Phys. Rev. B, 89 (2014) 165129.
[25] Y.S. Hou, H.J. Xiang, X.G. Gong, Intrinsic insulating ferromagnetism in manganese oxide thin films, Phys. Rev. B, 89 (2014) 064415.
[26] B.R.K. Nanda, S. Satpathy, Magnetic and orbital order inLaMnO3under uniaxial strain: A model study, Phys. Rev. B, 81 (2010) 174423.
[27] E. Pavarini, E. Koch, Origin of Jahn-Teller distortion and orbital order in LaMnO3, Phys. Rev. Lett., 104 (2010) 086402.
[28] A.M. Zhang, S.L. Cheng, J.G. Lin, X.S. Wu, Strain controlled orbital state and magnetization in insulating LaMnO3+δ films, J. Appl. Phys., 117 (2015) 17B325.
[29] J. Roqueta, A. Pomar, L. Balcells, C. Frontera, S. Valencia, R. Abrudan, B. Bozzo, Z. Konstantinović, J. Santiso, B. Martínez, Strain-Engineered Ferromagnetism in LaMnO3Thin Films, Crystal Growth & Design, 15 (2015) 5332-5337.
[30] S. El-Khatib, S. Bose, C. He, J. Kuplic, M. Laver, J.A. Borchers, Q. Huang, J.W. Lynn, J.F. Mitchell, C. Leighton, Spontaneous formation of an exchange-spring composite via magnetic phase separation inPr1−xCaxCoO3, Phys. Rev. B, 82 (2010) 100411 (R).
[31] T. Chatterji, F. Fauth, B. Ouladdiaf, P. Mandal, B. Ghosh, Volume collapse inLaMnO3caused by an orbital order-disorder transition, Phys. Rev. B, 68 (2003) 052406.
[32] R. Zhao, K. Jin, Z. Xu, H. Guo, L. Wang, C. Ge, H. Lu, G. Yang, The oxygen vacancy effect on the magnetic property of the LaMnO3−δ thin films, Appl. Phys. Lett., 102 (2013) 122402.
[33] A.N. Ulyanov, D.S. Yang, N. Chau, S.C. Yu, S.I. Yoo, Divalent manganese in A-position of perovskite cell: X-ray absorption finite structure study of La0.6Sr0.4−xMnTixO3 manganites, J. Appl. Phys., 103 (2008) 07F722.
[34] I. Marozau, P.T. Das, M. Döbeli, J.G. Storey, M.A. Uribe-Laverde, S. Das, C. Wang, M. Rössle, C. Bernhard, Influence of La and Mn vacancies on the electronic and magnetic properties ofLaMnO3thin films grown by pulsed laser deposition, Phys. Rev. B, 89 (2014) 174422.
[35] J. Nogues, I.K. Schuller, Exchange bias, J. Magn. Magn. Mater., 192 (1999) 203-232.
[36] N. Moutis, C. Christides, I. Panagiotopoulos, D. Niarchos, Exchange-coupling properties of La1-xCaxMnO3 ferromagnetic/antiferromagnetic multilayers, Phys. Rev. B, 64 (2001) 094429.
[37] S.-S. Yan, J.A. Barnard, F.-T. Xu, J.L. Weston, G. Zangari, Critical dimension of the transition from single switching to an exchange spring process in hard/soft exchange-coupled bilayers, Phys. Rev. B, 64 (2001) 184403.
[38] A.N. Dobrynin, D. Givord, Exchange bias in a Co/CoO/Co trilayer with two different ferromagnetic-antiferromagnetic interfaces, Phys. Rev. B, 85 (2012) 014413.

[39] P. Yu, J.S. Lee, S. Okamoto, M. Rossell, M. Huijben, C.H. Yang, Q. He, J. Zhang, S. Yang, M. Lee, Q. Ramasse, R. Erni, Y.H. Chu, D. Arena, C.C. Kao, L. Martin, R. Ramesh, Interface Ferromagnetism and Orbital Reconstruction in BiFeO3/La0.7Sr0.3MnO3 Heterostructures, Phys. Rev. Lett., 105 (2010) 027201.
[40] J.F. Ding, O.I. Lebedev, S. Turner, Y.F. Tian, W.J. Hu, J.W. Seo, C. Panagopoulos, W. Prellier, G. Van Tendeloo, T. Wu, Interfacial spin glass state and exchange bias in manganite bilayers with competing magnetic orders, Phys. Rev. B, 87 (2013) 054428.
[41] X.H. Huang, J.F. Ding, G.Q. Zhang, Y. Hou, Y.P. Yao, X.G. Li, Size-dependent exchange bias inLa0.25Ca0.75MnO3nanoparticles, Phys. Rev. B, 78 (2008) 224408.
[42] R. Skomski, J.M.D. Coey, Giant energy product in nanostructured two-phase magnets, Phys. Rev. B, 48 (1993) 15812-15816.
[43] J.S. Jiang, E.E. Fullerton, M. Grimsditch, C.H. Sowers, S.D. Bader, Exchange-spring behavior in epitaxial hard/soft magnetic bilayer films, J. Appl. Phys., 83 (1998) 6238-6240.
[44] C. Binek, S. Polisetty, X. He, A. Berger, Exchange bias training effect in coupled all ferromagnetic bilayer structures, Phys. Rev. Lett., 96 (2006) 067201.
[45] B. Li, R.V. Chopdekar, E. Arenholz, A. Mehta, Y. Takamura, Unconventional switching behavior in La0.7Sr0.3MnO3/La0.7Sr0.3CoO3 exchange-spring bilayers, Appl. Phys. Lett., 105 (2014) 202401.
[46] E. Dagotto, T. Hotta, A. Moreo, Colossal magnetoresistant materials the key role of phase separation, Phys. Rep., 344 (2001) 1.
[47] M. Uehara, S. Mori, C.H. Chen, S.W. Cheong, Percolative phase separation underlies colossal magnetoresistance in mixed-valent manganites, Nature, 399 (1999) 560-563.
[48] A.S. Moskvin, Disproportionation and electronic phase separation in parent manganiteLaMnO3, Phys. Rev. B, 79 (2009) 115102.
[49] J.H. Lee, K.T. Delaney, E. Bousquet, N.A. Spaldin, K.M. Rabe, Strong coupling of Jahn-Teller distortion to oxygen-octahedron rotation and functional properties in epitaxially strained orthorhombic LaMnO3, Phys. Rev. B, 88 (2013) 174426.
[50] K.H. Ahn, A.J. Millis, Effects of uniaxial strain inLaMnO3, Phys. Rev. B, 64 (2001) 115103.
[51] X.R. Wang, C.J. Li, W.M. Lü, T.R. Paudel, D.P. Leusink, M. Hoek, N. Poccia, A. Vailionis, T. Venkatesan, J.M.D. Coey, E.Y. Tsymbal, Ariando, H. Hilgenkamp, Imaging and control of ferromagnetism in LaMnO3-SrTiO3 heterostructures, Science, 349 (2015) 716.
[52] X. Zhai, L. Cheng, Y. Liu, C.M. Schleputz, S. Dong, H. Li, X. Zhang, S. Chu, L. Zheng, J. Zhang, A. Zhao, H. Hong, A. Bhattacharya, J.N. Eckstein, C. Zeng, Correlating interfacial octahedral rotations with magnetism in (LaMnO3+delta)N/(SrTiO3)N superlattices, Nat Commun, 5 (2014) 4283.
[53] E.E. Fullerton, J.S. Jiang, S.D. Bader, Hard-soft magnetic heterostructures： model exchange-spring magnets, J. Magn. Magn. Mater., 200 (1999) 392.
[54] F. Tsui, M.C. Smoak, T.K. Nath, C.B. Eom, Strain-dependent magnetic phase diagram of epitaxial La0.67Sr0.33MnO3 thin films, Appl. Phys. Lett., 76 (2000) 2421-2423.
[55] G. Shirane, Y. Yamada, Lattice-Dynamical Study of the 110°K Phase Transition in SrTiO3, Phys. Rev., 177 (1969) 858-863.
[56] Y.K. Liu, Y.P. Yao, S.N. Dong, S.W. Yang, X.G. Li, Effect of magnetic field on ferroelectric properties of BiFeO3/La5/8Ca3/8MnO3 epitaxial heterostructures, Phys. Rev. B, 86 (2012) 075113.
[57] V.K. Vlasko-Vlasov, Y.K. Lin, D.J. Miller, U. Welp, G.W. Crabtree, V.I. Nikitenko, Direct Magneto-Optical Observation of a Structural Phase Transition in Thin Films of Manganites, Phys. Rev. Lett., 84 (2000) 2239.
[58] U. Gebhardt, N.V. Kasper, A. Vigliante, P. Wochner, H. Dosch, F.S. Razavi, H.U. Habermeier, Formation and thickness evolution of periodic twin domains in manganite films grown on SrTiO3(001) substrates, Phys. Rev. Lett., 98 (2007) 096101.